Spectrochimica Acta Part A 79 (2011) 476–480

Contents lists available at ScienceDirect

Spectrochimica Acta Part A: Molecular and Biomolecular Spectroscopy

journal homepage: www.elsevier.com/locate/saa

EPR and photoluminescence studies of ZnO:Mn nanophosphors prepared by solution combustion route

A. Jagannatha Reddy[a], M.K. Kokila[b], H. Nagabhushana[c,*], J.L. Rao[d], B.M. Nagabhushana[e], C. Shivakumara[f], R.P.S. Chakradhar[g,**]

[a] Department of Physics, M. S. Ramaiah Institute of Technology, Bangalore 560 054, India
[b] Department of Physics, Bangalore University, Bangalore 560 056, India
[c] Centre for Nanoscience Research (CNR), Tumkur University, Tumkur 572 103, India
[d] Department of Physics, S.V. University, Tirupathi 517 502, India
[e] Department of Chemistry, M. S. Ramaiah Institute of Technology, Bangalore 560 054, India
[f] Solid State and Structural Chemistry Unit, Indian Institute of Science, Bangalore 560 012, India
[g] Central Glass and Ceramic Research Institute (CSIR), Kolkata 700 003, India

ARTICLE INFO

Article history:
Received 29 October 2010
Received in revised form 22 February 2011
Accepted 9 March 2011

Keywords:
ZnO:Mn
Diluted magnetic semiconductor (DMS)
Electron paramagnetic resonance (EPR)
Luminescence

ABSTRACT

Nanocrystalline ZnO:Mn (0.1 mol%) phosphors have been successfully prepared by self propagating, gas producing solution combustion method. The powder X-ray diffraction of as-formed ZnO:Mn sample shows, hexagonal wurtzite phase with particle size of ~40 nm. For Mn doped ZnO, the lattice parameters and volume of unit cell (a = 3.23065 Å, c = 5.27563 Å and V = 47.684 (Å)^3) are found to be greater than that of undoped ZnO (a = 3.19993 Å, c = 5.22546 Å and V = 46.336 (Å)^3). The SEM micrographs reveal that besides the spherical crystals, the powders also contained several voids and pores. The TEM photograph also shows the particles are approximately spherical in nature. The FTIR spectrum shows two peaks at ~3428 and 1598 cm^{-1} which are attributed to O–H stretching and H–O–H bending vibration. The PL spectra of ZnO:Mn indicate a strong green emission peak at 526 nm and a weak red emission at 636 nm corresponding to $^4T_1 \rightarrow {}^6A_1$ transition of Mn^{2+} ions. The EPR spectrum exhibits fine structure transition which will be split into six hyperfine components due to ^{55}Mn hyperfine coupling giving rise to all 30 allowed transitions. From EPR spectra the spin-Hamiltonian parameters have been evaluated and discussed. The magnitude of the hyperfine splitting (A) constant indicates that there exists a moderately covalent bonding between the Mn^{2+} ions and the surrounding ligands. The number of spins participating in resonance (N), its paramagnetic susceptibility (χ) have been evaluated.

© 2011 Elsevier B.V. All rights reserved.

1. Introduction

ZnO is a key n-type II–VI technological semiconductor with characteristic features, such as large band gap (3.37 eV), low power threshold for optical pumping and highly efficient UV emission resulting from a large exciton binding energy (60 meV) at room temperature. The lack of a center of symmetry in wurtzite, combined with large electromechanical coupling, results in strong piezoelectric and pyroelectric properties and the consequent use of ZnO in mechanical actuators and piezoelectric sensors. ZnO has also been used in a wide range of applications such as transparent conductive electrodes, gas sensors, solar cells, opto-electronic devices, surface-acoustic waveguides and field emission devices [1–4].

For the emerging scientific field of spintronics [5], materials which can provide spin-polarized charge currents for spin injection into semiconductors are required. As potential candidates, diluted magnetic semiconductors (DMSs) have attracted a great deal of interest. DMSs are conventional semiconductor (for e.g. ZnO) doped with transition metal (TM) or rare-earth elements which are randomly distributed on substitutional lattice sites and Ferro magnetically aligned via an indirect magnetic coupling [6–8]. Transition metal doped ZnO is one of the most promising DMS candidates as it is predicted to be ferromagnetic above room temperature.

Various techniques have been used to synthesize pure or TM doped ZnO nano materials [9]. Searching new methodology to synthesize uniform nano-sized ZnO particles is of great importance for both fundamental study and practical application, and thus different methods such as thermal decomposition; chemical vapor deposition, sol–gel, spray pyrolysis, solution combustion and precipitation have still been developed for the fabrica-

* Corresponding author.
** Corresponding author. Present address: Scientist (CSIR-NAL), Bangalore 560 017, India. Tel.: +91 80 25086251.
E-mail addresses: bhushanvl@rediffmail.com (H. Nagabhushana), sreechakra72@yahoo.com (R.P.S. Chakradhar).

1386-1425/$ – see front matter © 2011 Elsevier B.V. All rights reserved.
doi:10.1016/j.saa.2011.03.014

tion of nano-sized ZnO particles with uniform morphology and size.

In the present study, Mn doped ZnO nano powders have been synthesized by solution combustion method. This method has been found to be unique to obtain high surface area fine particles. It involves rapid heating of an aqueous redox mixture containing stoichiometric amounts of corresponding metal nitrates and hydrazine based fuels [10,11]. Therefore, the authors are interested to synthesize Mn-doped ZnO nano powders by solution combustion process. The prepared nano powders have been characterized by powder X-ray diffraction (PXRD), scanning electron microscopy (SEM), transmission electron microscopy (TEM) and Fourier transform infrared spectroscopy (FT-IR). Photoluminescence (PL) and electron paramagnetic resonance (EPR) studies have also been performed on the prepared phosphors.

2. Experimental

2.1. Synthesis

The starting chemicals used in the present study were $Zn(NO_3)_2$, $Mn(NO_3)_2$ and $C_2H_6N_4O_2$ (oxalyldihydrazide) in the mole ratio 1.0:0.01:1.0 and dissolved in minimum quantity of water in a cylindrical petri dish. The dish containing the redox mixture was introduced into a muffle furnace maintained at $300 \pm 10\,^{\circ}C$. Initially the solution boiled with frothing and foaming and underwent dehydration. At the point of complete dehydration, the surface ignited, burning with a flame (~1000 °C) and yielding a voluminous solid product within 5 min. These compounds were prepared in an open muffle furnace kept in a fume cupboard with exhaust.

2.2. Characterization

The powder X-ray diffraction studies were carried out using Phillips X-ray diffractometer (model PW 3710) with Cu Kα radiation (λ = 1.5405 Å). The surface morphology of the samples was examined using Scanning electron microscopy (SEM) (JEOL JSM 840A). Transmission electron microscopy (TEM) analysis was performed on a Hitachi H-8100 (accelerating voltage up to 200 kV, LaB_6 filament) equipped with EDS (Kevex Sigma TM Quasar, USA). The photoluminescence studies were carried out using a Perkin–Elmer LS-55 luminescence spectrophotometer equipped with Xe lamp (excitation wavelength 250 nm). The EPR spectra were recorded at room temperature using a JEOL-FE-1X EPR spectrometer operating in the X-band frequency (≈9.205 GHz) with a field modulation frequency of 100 kHz. The magnetic field was scanned from 220 to 420 mT and the microwave power used was 10 mW. A powdered specimen of 100 mg was taken in a quartz tube for EPR measurements.

3. Results and discussion

3.1. Powder X-ray diffraction (PXRD)

Fig. 1 shows the powder X-ray diffraction (PXRD) profile of ZnO:Mn nano powder. The X-ray diffraction peaks have been indexed (JCPDS 36-1451) and found to be in hexagonal wurtzite structure. The PXRD profiles demonstrate eight prominent peaks, indicating a non-preferential orientation, and it is evident that those peaks correspond to the wurtzite structure. No trace of manganese oxide or any binary zinc manganese phase has been observed which confirms that Mn is doped into ZnO matrix by substituting Zn. Thus, it is clear that the formed $Zn_{0.99}Mn_{0.01}O$ is a singular phase, its formation is complete at the furnace temperature, and a further calcination treatment was not necessary. A

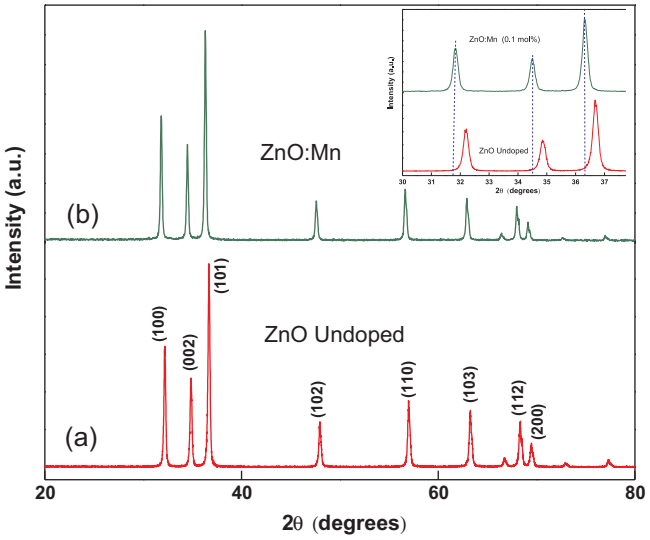

Fig. 1. PXRD of (a) undoped and (b) Mn doped ZnO (inset: shift of main peaks).

small shift in the position of main peaks to the lower side of 2θ values is observed for Mn doped sample. This observation is similar to the case in transition metal (Fe, Cu and Ni) doped ZnO studied by Ekambaram et al. [12]. This shift is mainly due to the larger ionic radius of Mn^{2+} (0.83 Å) than that of tetrahedral ionic radius of Zn^{2+} (0.74 Å). This indicates that the doped Mn atoms substitute Zn atoms.

The lattice parameters for hexagonal ZnO and Mn-doped ZnO nanoparticles were estimated from the equation:

$$\frac{1}{d_{hkl}^2} = \frac{4}{3}\left(\frac{1}{a^2}\right) + \frac{1}{c^2} \quad (1)$$

where a and c are the lattice parameters (being hexagonal $c/a = \sqrt{8/3}$) and d_{hkl} is the interplaner spacing for the plane of Miller indices ($h\,k\,l$). The volume of the unit cell for a hexagonal system has been calculated from the following equation:

$$V = 0.866 \times a^2 \times c \quad (2)$$

For Mn doped ZnO, the lattice parameters and volume of unit cell (a = 3.23065 Å, c = 5.27563 Å and V = 47.684 (Å)^3) are found to be greater than that of undoped ZnO (a = 3.19993 Å, c = 5.22546 Å and V = 46.336 (Å)^3) which follow the Vegard's law [13,14]. Therefore, the Mn ions are understood to have occupied the Zn sites without changing its wurtzite structure.

The average crystallite size (D) was estimated from the Debye–Scherrer's equation,

$$D = \frac{0.9\lambda}{\beta\,\cos\theta} \quad (3)$$

where λ represents the wavelength of the X-ray radiation, β is the full width at half maximum of diffraction peak (in rad) and θ is the scattering angle. The crystallite size was found to be in the range ~40 nm.

3.2. Scanning electron microscopy (SEM)

Fig. 2 shows the SEM images of Mn doped ZnO nanocrystalline powder. The micrographs revealed that the primary particles are uniform, circular in shape and weakly agglomerated. Besides the spherical crystals, several voids and pores are observed in all images because of the escaping gases during combustion reaction. Magnified view shows the presence of pores of diameter close to 500 nm with several particles in the size range of 100–150 nm nearby.

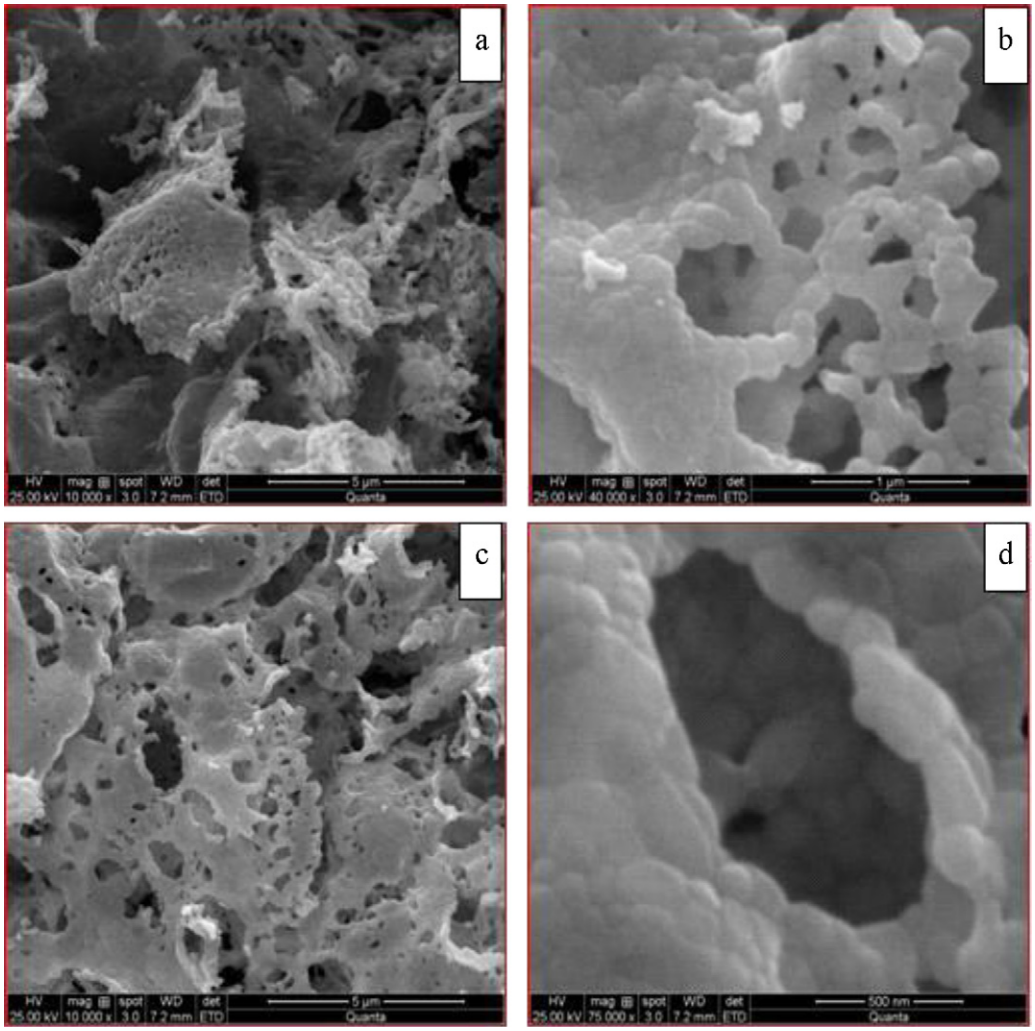

Fig. 2. SEM micrographs of Mn doped ZnO at different magnifications.

When gas is escaping with high pressure, pores are formed with the simultaneous formation of small particles. The morphology of the powders reflects the inherent nature of the combustion process.

3.3. Transmission electron microscopy (TEM)

TEM observation and selective area electron diffraction (SAED) were carried out to study the crystalline characteristics of the nanoparticles. The TEM photograph of Mn doped ZnO is given in Fig. 3. It indicates that the ZnO particles are approximately spherical and the average diameter of the particles is ~40 nm. This is in good agreement with the value obtained from Scherrer's formula. In addition, a fraction of the ZnO nano-sized particles being in the form of aggregates shown in Fig. 3 also agree with those obtained from the SEM image in Fig. 2. The corresponding SAED pattern (inset of Fig. 3) confirms that the nanoparticles are wurtzite single crystalline in nature.

3.4. Fourier transformed infrared spectroscopy (FT-IR)

The composition, quality and molecular structure of the product were analyzed by the FTIR spectroscopy. Fig. 4 shows the FT-IR spectrum of the undoped ZnO and 0.1 mol% Mn doped ZnO nanocrystalline powder which was acquired in the range of 400–4000 cm^{-1}. The two peaks at ~3428 and 1598 cm^{-1} are attributed to O–H stretching vibration and H–O–H bending vibration, which are assigned to small amount of H_2O existing in the nanocrystalline ZnO. The peak at 427 cm^{-1} is ascribed to Zn–O stretching vibration.

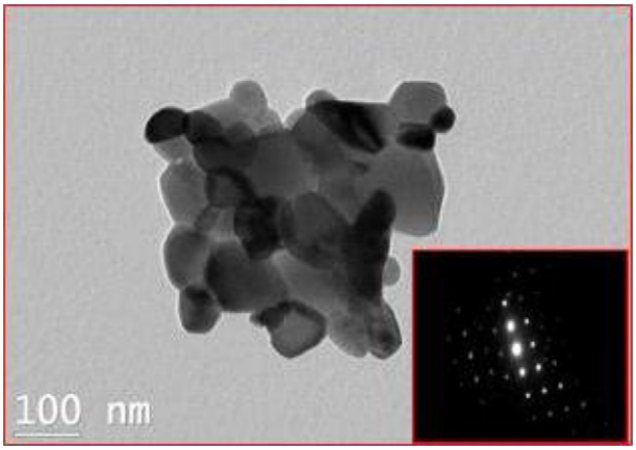

Fig. 3. TEM micrograph of Mn doped ZnO (inset: SAED pattern).

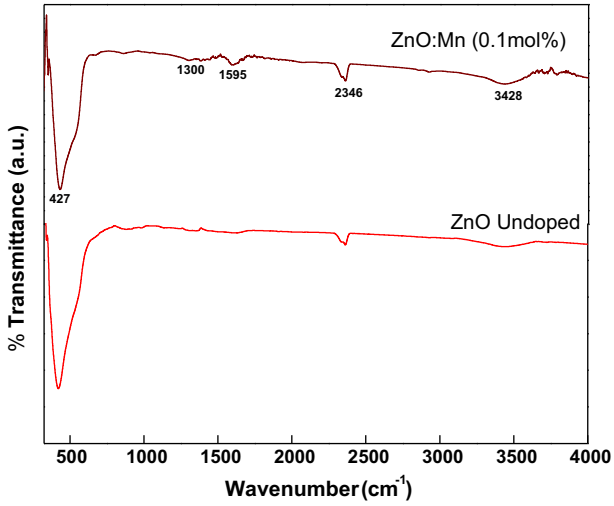

Fig. 4. FTIR spectrum of undoped and Mn doped ZnO.

3.5. Photoluminescence (PL)

The PL spectra of ZnO:Mn shown in Fig. 5, indicate a strong green emission peak at 526 nm for excitation at 412 nm, while the excitation spectrum corresponding to this emission shows peaks at 396 nm, 412 nm, 432 nm and 446 nm. The luminescent properties of the nanopowders are strongly dependent on the crystal structure of host materials. The PL of ZnO:Mn nano powder has been characterized by the transitions of $3d^5$ of Mn^{2+} ions acting as an activating center. In a cubic crystal field of low to moderate strength, the five d electrons of Mn^{2+} ions are distributed in the t_2 and e orbitals, with three in the former and two in the latter. Thus, the ground state configuration is $(t_2)^3\,(e)^2$. This configuration gives rise to the electronic states, $^6A_1$, $^4A_1$, ^4E, $^4T_1$, and $^4T_2$, and to a number of doublet states of which $^6A_1$ lies in the lowest according to Hund's rule. Since all the excited states of Mn^{2+} ion (belonging to d^5 configuration) will be either quartets or doublets, the luminescence spectra of Mn^{2+} ions will have only spin forbidden transitions. The observed excitation peaks in the present study at 396 nm, 412 nm, 432 nm and 446 nm can be attributed to the transitions from $^6A_1 \rightarrow {}^4T_2$ (D), $^6A_1 \rightarrow {}^4A_1$, ^4E (G), $^6A_1 \rightarrow {}^4T_2$ (G) and $^6A_1 \rightarrow {}^4T_1$ (G) respectively.

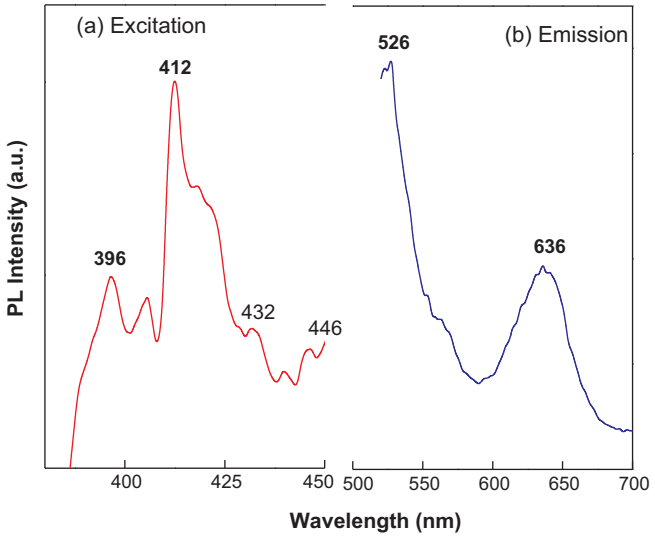

Fig. 5. PL spectrum of Mn doped ZnO (a) excitation spectrum and (b) emission spectrum.

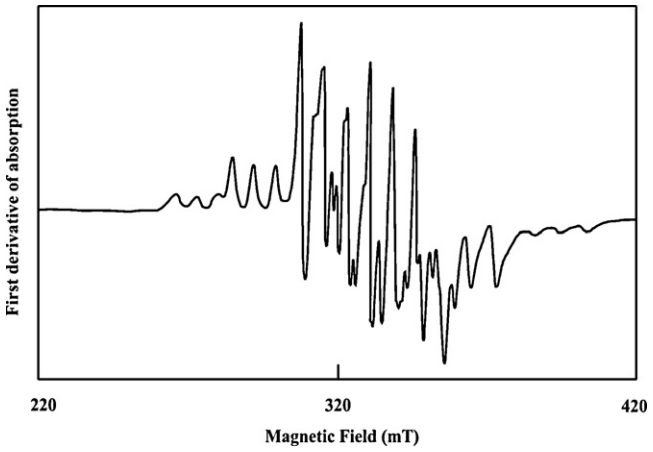

Fig. 6. EPR spectrum of Mn doped ZnO.

The luminescence behaviors of the Mn^{2+} activator have been extensively studied by many researchers [15]. According to the reports, the emission of the Mn^{2+} activator depends on the crystal environment. The tetrahedrally coordinated Mn^{2+} ion gives a green emission by forming a weak crystal field, while the octahedrally coordinated Mn^{2+} ion exhibits an orange-to-red emission at the liquid nitrogen temperature by forming a strong crystal field [16]. In the present study, the emission at 526 nm (19,006 cm^{-1}) is typical green emission. The emission process from this material is attributed to a d-level spin-forbidden transition for the Mn^{2+} ions acting as an activating center. In particular, the transition from the lowest excited state to the ground state, $^4T_1 \rightarrow {}^6A_1$, is directly responsible for the green light emission and is arising from the tetrahedrally coordinated Mn^{2+} sites. In Fig. 5(b) the luminescence peaking at 636 nm (15,719 cm^{-1}) may come from Mn^{2+} ions in a different site. The intensity of green emission is more compared to red emission suggesting that more number of Mn ions is in tetrahedral sites.

3.6. Electron paramagnetic resonance (EPR)

Fig. 6 shows the EPR spectrum of Mn^{2+} ions in ZnO:Mn nano powder recorded at room temperature. Mn^{2+} ion, is unique among d^n configurations and there is only one state with maximum spin multiplicity ($^6S_{5/2}$) which splits into three Kramers doublets ($\pm5/2$, $\pm3/2$ and $\pm1/2$). In the presence of magnetic field, the degeneracy is completely removed and five fine structure transitions are possible. Each fine structure transition will be split into six hyperfine components due to ^{55}Mn hyperfine coupling and may give in all 30 allowed transitions. The sextets belong to the transitions $5/2 \leftrightarrow 3/2$, $3/2 \leftrightarrow 1/2$, $1/2 \leftrightarrow -1/2$, $-1/2 \leftrightarrow -3/2$, $-3/2 \leftrightarrow -5/2$.

The EPR spectrum of powder sample was analyzed in order to obtain spin-Hamiltonian parameters. The following spin-Hamiltonian has been taken into account [17].

$$H = \beta \text{B.g.s} + D\left[S_z^2 - \left\{\frac{S(S+1)}{3}\right\}\right] + \text{I.A.S} \quad (4)$$

where the first term represents the electronic Zeeman term, second term characterize the zero-field splitting of the sextet ground state. The sextet observed at the central transition corresponding to $1/2 \leftrightarrow -1/2$ transition has a g value of $g \approx 1.978$. The sextet observed has been analyzed using the following expressions [18] for resonance fields. From the observed spin-Hamiltonian parameters it is concluded that the site symmetry around the central metal ion is distorted tetrahedron.

The ability to observe the ^{55}Mn hyperfine structure has two tangible benefits. (1) It generally allows unambiguous assignments

of positions of complex resonance lines to manganese and (2) the magnitude of the hyperfine splitting constant provides a measure of the bonding between Mn^{2+} ions and its surrounding ligands [19,20]. The average hyperfine splitting constant A_{avg} evaluated in the present study is found to be 80 G. The strength of the hyperfine splitting (A) depends on the matrix into which the ion is dissolved and is mainly determined by the electronegativity of the neighbours. This means a qualitative measure of the covalency of the bonding in the matrix which can be determined from the value of A; the smaller the splitting, the more covalent the bonding of the anion. The magnitude of the hyperfine splitting constant (A) in the present study indicates that there exists a moderately covalent bonding between Mn^{2+} ions and the surrounding ligands.

The number of spins participating in resonance can be calculated by comparing the area under the absorption curve with that of a standard ($CuSO_4{\cdot}5H_2O$ in this study) of known concentration. Weil et al. [21] gave the following expression which includes the experimental parameters of both sample and standard.

$$N = \frac{A_x(Scan_x)^2 G_{std}(B_m)_{std}(g_{std})^2[S(S+1)]_{std}(P_{std})^{1/2}}{A_{std}(Scan_{std})^2 G_x(B_m)_x(g_{std})^2[S(S+1)]_x(P_x)^{1/2}}[std] \quad (5)$$

where A is the area under the absorption curve, which can be obtained by double integrating the first derivative EPR absorption curve, *scan* is the magnetic field corresponding to a unit length of the chart, G is the gain, B_m is the modulation field width, g is the g factor, S is the spin of the system in its ground state. P is the power of the microwave source. The subscripts '*x*' and '*std*' represent the corresponding quantities for the ZnO:Mn^{2+} nanophosphor and the reference ($CuSO_4{\cdot}5H_2O$) respectively. The value of N has been calculated for the ZnO:Mn^{2+} nanophosphor at room temperature and it is found to be 5.17×10^{19}. The EPR data can be used to calculate the paramagnetic susceptibility of the sample using the formula [22].

$$\chi = \frac{Ng^2\beta^2 J(J+1)}{3k_BT} \quad (6)$$

where N is the number of spins per m^3 and the other symbols have their usual meaning. N can be calculated from Eq. (5) and g is taken from EPR data. The paramagnetic susceptibility (χ) evaluated from EPR data for ZnO:Mn (0.1 mol%) nano powder is found to be $1.23 \times 10^{-5}\ m^3\ kg^{-1}$. We chose to determine the spin susceptibility from EPR, because this technique has several advantages over a static measurement, where a diamagnetic contribution must be subtracted off.

4. Conclusions

Mn-doped ZnO nanophosphor has been synthesized successfully by the solution combustion process. Compared to the solid-state reaction method, combustion synthesis has outstanding potential for producing transition metal doped ZnO nanophosphor. The powder X-ray diffraction of as-formed ZnO:Mn sample shows completely crystalline, hexagonal wurtzite phase with a particle size of about ~40 nm. SEM micrographs show that the primary particles are uniform, circular in shape and weakly agglomerated. TEM results also confirm the phosphor particles are of nano size. The PL spectrum shows a strong green emission peak at 526 nm and a weak red emission at 636 nm corresponding to $^4T_1 \rightarrow {}^6A_1$ transition of Mn^{2+} ions. EPR spectra of ZnO:Mn exhibit hyperfine structure due to interaction of electron spin ($S = 5/2$) with its nuclear spin ($I = 5/2$) and the each fine structure transition which will be split into six hyperfine components due to ^{55}Mn hyperfine coupling and giving rise to all 30 allowed transitions. The sextets belong to the transitions $5/2 \leftrightarrow 3/2$, $3/2 \leftrightarrow 1/2$, $1/2 \leftrightarrow -1/2$, $-1/2 \leftrightarrow -3/2$, $-3/2 \leftrightarrow -5/2$. In the present study the occurrence of not more than 30 lines suggest that Mn^{2+} ions in this lattice occupies the metal site (Zn). The observed hyperfine splitting constant A, indicates that the bonding between the Mn^{2+} ions and the surrounding ligands is moderately covalent in nature.

Acknowledgements

Dr. B.M Nagabhushana gratefully acknowledges Visvesvaraya Technological University, Belgaum, for the financial support (VTU/2009-10/A-9/11714) to carryout this research work. Dr. H. Nagabhushana thanks Dr. S. C. Sharma, Vice-chancellor, Tumkur University, Tumkur, for constant encouragement and support.

References

[1] S.K. Marathe, P.M. Koinkar, S.S. Ashtaputre, M.A. More, S.W. Gosavi, D.S. Joag, S.K. Kulkarni, Nanotechnology 17 (2006) 1932–1936.
[2] S. Liu, F. Liu, Z. Wang, Chem. Phys. Lett. 343 (2005) 489–492.
[3] F. Gu, S.F. Wang, M.K. Lu, G.Z. Zhou, D. Xu, D.R. Yuan, Langmuir 20 (2004) 3528–3531.
[4] T. Schmidt, G. Muller, L. Spanhel, Chem. Mater. 10 (1998) 65–71.
[5] S.A. Wolf, D.D. Awschalom, R.A. Buhrman, J.M. Daughton, S. von Molnar, M.L. Roukes, A.Y. Chtchelkanova, D.M. Treger, Science 294 (2001) 1488–1495.
[6] K.R. Kittilstved, D.R. Gamelin, J. Am. Chem. Soc. 127 (2005) 5292–5293.
[7] C. Song, S.N. Pan, X.J. Liu, X.W. Li, F. Zeng, W.S. Yan, B. He, F. Pan, J. Phys. Condens. Matter. 19 (2007) 176229.
[8] F. Pan, C. Song, X. Liu, Y. Yang, F. Zeng, Mater. Sci. Eng. R 62 (2008) 1–35.
[9] B.Q. Wang, P.W. Wang, X.J. Zhang, X.Z. Zhang, H.G. Fu, L.Q. Jing, D.P. Yu, Chin. J. Inorg. Chem. 23 (2007) 1365.
[10] J.J. Kingsley, K.C. Patil, Mater. Lett. 6 (1988) 427–432.
[11] B.M. Nagabhushana, R.P.S. Chakradhar, K.P. Ramesh, V. Prasad, C. Shivakumara, G.T. Chandrappa, Philos. Mag. 90 (2010) 2009–2025.
[12] S. Ekambaram, Y. Iikubo, A. Kudo, J. Alloys Compd. 433 (2006) 237–240.
[13] L. Vegard, Z. Phys. 5 (1921) 17–26.
[14] A.R. Denton, N.W. Ashcroft, Phys. Rev. A 43 (1991) 3161–3164.
[15] D.T. Palumbo, J.J. Brown Jr., J. Elctrochem. Soc. 117 (1970) 1184–1188.
[16] V. Singh, R.P.S. Chakradhar, J.L. Rao, D.-K. Kim, J. Lumin. 128 (2008) 1474–1478.
[17] A. Abragam, B. Bleaney, Electron Paramagnetic Resonance of Transition Ions, Clarendon, Oxford, 1970.
[18] R. Aasa, J. Chem. Phys. 52 (1970) 3919–3930.
[19] J.S. Van Wieringen, Discuss. Faraday Soc. 19 (1955) 118–126.
[20] F.D. Tsay, L. Helmholz, J. Chem. Phys. 50 (1969) 2642–2650.
[21] J.A. Weil, J.R. Bolton, J.E. Wertz, Electron Paramagnetic Resonance-Elementary Theory and Practical Applications, Wiley, New York, 1994, p. 498.
[22] N.W. Aschcroft, N.D. Mermin, Solid State Physics, Harcourt College Publishers, 2001, p. 656.